



HELLENIC REPUBLIC  
National and Kapodistrian  
University of Athens  
Department of Biology



Athens International  
Master's Programme  
in Neurosciences

---

Department of Medicine  
Aristotle University of Thessaloniki

---

## RESEARCH THESIS PROJECT

Analyzing spontaneous oscillatory activity and network organization  
in cortical slices using the genetically encoded voltage indicator ArcLight

SPYRIDON ANTONIADIS

Student ID: 7113112000003

2023



HELLENIC REPUBLIC  
National and Kapodistrian  
University of Athens  
Department of Biology



Athens International  
Master's Programme  
in Neurosciences

Department of Medicine  
Aristotle University of Thessaloniki

## RESEARCH THESIS PROJECT

Analyzing spontaneous oscillatory activity and network organization  
in cortical slices using the genetically encoded voltage indicator ArcLight

### Three Member Evaluation Committee

**Supervisor: Kosmidis Efstratios, Associate Professor**

Department of Medicine, Aristotle University of Thessaloniki, Thessaloniki, Greece

**Thesis reviewer: Skaliora Irimi, Professor**

Department of History and Philosophy of Science, National and Kapodistrian University of Athens,  
Athens, Greece

Centre for Basic Research, Biomedical Research Foundation of the Academy of Athens, Athens,  
Greece

**Thesis reviewer: Cutsuridis Vassilis, Senior Lecturer**

School of Computer Science, University of Lincoln, Lincoln, United Kingdom

2023

# Analyzing spontaneous oscillatory activity and network organization in cortical slices using the genetically encoded voltage indicator ArcLight

**Antoniadis Spyridon**

Athens International Master's Programme in Neurosciences, Department of Biology, National and Kapodistrian University of Athens, Athens, Greece

Department of Medicine, Aristotle University of Thessaloniki, Thessaloniki, Greece

Email: santonia@biol.uoa.gr

**Supervisor: Kosmidis Efstratios, Associate Professor**

Department of Medicine, Aristotle University of Thessaloniki, Thessaloniki, Greece

Email: kosmidief@med.auth.gr

## Summary

Genetically encoded voltage indicators (GEVIs) have been praised as a potential pinnacle in the field of neuroscience, yet their significant impact on our understanding of circuit physiology remains elusive. In addition, analyzing GEVI datasets poses a significant challenge as these datasets are large and there is no consensus on a specific method of analysis. Here, by expressing the GEVI ArcLight pan-neuronally we were able to optically resolve bicuculline induced spontaneous oscillations in brain slices of the mouse motor cortex. We next sought to analyze the emerged dataset under a network theory perspective, exploiting its ability to uncover complex relationships and reveal emergent properties within the interconnected elements, with our aim being to study whether the spontaneous occurrence of an oscillation can be predicted based on the imaged network activity. Our analysis suggests that alternative interdisciplinary intuitions about the functional interpretation of the data might be more appropriate, at least until the inherent technical limitations surrounding GEVIs are finally resolved.

## Keywords

ArcLight, genetically encoded voltage indicators, optical recordings, motor cortex, neural population activity, oscillations, functional network organization

## Highlights

Successful detection of bicuculline-induced spontaneous oscillations using ArcLight

Data exploratory analysis under a network theory perspective

## Introduction

Genetically encoded voltage indicators (GEVIs), chimeric proteins that sense and optically report changes in membrane potential, represent a valuable tool for enabling the study of neuronal activity with high spatiotemporal resolution (Xu et al., 2017; Bando et al., 2019; Dong et al., 2022). In contrast to their counterparts, calcium indicators, i.e., fluorescent molecules that rely on intracellular calcium levels as a proxy for neuronal firing (Mank and Griesbeck, 2008; Grienberger and Konnerth, 2012; Dong et al., 2022), GEVIs offer several notable advantages: they are capable of

reporting subthreshold events including neuronal inhibition (Jin et al., 2012; Piatkevich et al., 2018; Bando et al., 2019), a crucial task for understanding the dynamics of neural circuits; they restrict voltage sensor expression to specific cell types using transgenic cre-recombinase mouse lines, allowing the experimenter to target distinct cell populations and elucidate the functional roles of different neuronal types within complex networks (Nakajima et al., 2016; Rhee et al., 2021; Platasa et al., 2022); finally, their rapid response kinetics make them well-suited for detecting fast neuronal events and investigating the intricacies of neuronal communication (Rhee et al., 2021).

Despite their advantages, GEVIs currently exhibit certain limitations, including a lower signal-to-noise ratio compared to their calcium counterparts, which can hinder the detection of neuronal activity in certain conditions. Additionally, they are prone to photobleaching, constraining both their utility for prolonged monitoring of membrane potential dynamics and their applicability for long-term studies (Yang and St-Pierre, 2016; Rhee et al., 2020).

ArcLight, a potent GEVI for *in vitro* and *in vivo* imaging, shows a near linear dynamic range over neuronal membrane physiological potentials, it is bright, and produces large optical signals in response to potential changes (Jin et al., 2012; Han et al., 2014; Lee et al. 2016). A recent independent comparison of different GEVIs demonstrated that ArcLight, even with expression limited to distinct cell types, gave the most consistent signal and was able to successfully report network activity, revealing distinct profiles for the excitatory and inhibitory cells in bicuculline-induced spontaneous oscillations of the motor cortex *ex vivo*, and thus hinting at their potentially divergent roles in oscillation propagation and onset mechanisms (Rhee et al., 2021).

Cortical oscillations are postulated to play a significant role in various cognitive functions due to their potential involvement in the synchronization of neuronal activity, which facilitates the integration and processing of information within and across distinct brain regions (Buzsáki, 2006; Wang, 2010; Buzsáki and Watson, 2012). Such synchronization facilitates the formation of dynamic, transient networks among spatially distributed neural populations. These networks, also known as cell assemblies or neural ensembles (Churchland and Sejnowski, 1992; Yuste, 2015; Carrillo-Reid et al., 2017), enable the coordination of information flow across various brain regions (Hopfield, 1982; Averbeck and Lee, 2004; Di Volo and Destexhe, 2021). The emergence of these assemblies is thought to be a key mechanism underlying the brain's capacity to engage in complex cognitive functions, such as attention, memory, and perception (Wallis, 2018; Nadeau, 2020). Furthermore, aberrant oscillatory patterns have been implicated in a variety of neurological disorders, including epilepsy, Parkinson's disease, and Tourette syndrome (Leckman et al., 2006; Mably and Colgin, 2018; Singh, 2018; Mendes et al., 2021; Neige et al., 2023).

The ability to predict spontaneous oscillatory neuronal activity by examining the underlying network activity holds immense potential for delving deeper into the complex dynamics underlying the emergence of this fundamental mechanism (Cabral et al. 2022), as well as potentially unveiling the existence of potential clusters of origin

for the induction of the voltage changes. This, in turn, would provide us with a powerful monitoring tool, paving the way for the development of more effective diagnostic and therapeutic strategies for neurological disorders such as Parkinson's disease and Tourette syndrome, where the ability to monitor both activation and inhibition is vital, as the balance between these two types of activities has been disrupted (Hirschmann et al., 2022).

Here, using a similar preparation as in (Rhee et al., 2021), we resort to network science techniques to study whether the spontaneous occurrence of an oscillation can be predicted based on the imaged network activity. Network science has emerged as a powerful framework for investigating the organization and function of the brain by conceptualizing it as a complex network of interacting components. This approach enables the quantitative analysis of brain connectivity at multiple scales, ranging from individual neurons and synapses to large-scale brain regions and systems (Bullmore and Sporns, 2009; Fornito et al., 2016; Bassett and Sporns, 2017; Sporns, 2018; Betzel, 2022), and has been recently used with success in the analysis of optical recordings as a data-driven information mining technique to achieve an unbiased comparison between recording conditions (Antoniadis, 2019; Nakajima et al., 2021).

To this end, three well-known functional network organization metrics were estimated and compared between several recording conditions during bicuculline-induced spontaneous oscillatory activity of the mouse motor cortex *ex vivo*. By assessing these metrics, we aimed to identify any discernible pattern in the functional network that could serve as a reliable predictor of future oscillatory events, with the working causal hypothesis being that the occurrence of such events must, in principle, be preceded by a detectable alteration in the underlying network dynamics, reflecting the reorganization of neuronal interactions within that network, as it anticipates a transition towards a different dynamical state (Pikovsky et al., 2001; Izhikevich, 2010; Fröhlich, 2015).

In summary, by combining the novel, exciting views of brain activity provided by the visualization of neuronal circuits with ArcLight, a recently developed GEVI, and the powerful framework of network theory, we sought to document the functional map of the mouse motor cortex during the emergence of bicuculline-induced spontaneous oscillations. The results presented here demonstrate that although ArcLight is a reliable GEVI for optically reporting neuronal circuit activity, and thus paving the way for reliable monitoring of both activation and inhibition, a purely exploratory network theoretic approach which considers the connectivity pattern of the imaged slice as a graph with nodes that are associated to pixels and a structure that reflects its functional organization falls short in capturing the intricate dynamics underlying spontaneous oscillatory activity, suggesting, in turn, that other data learning algorithms might be more appropriate in capturing its crucial aspects.

## Materials and methods

### Animals

Ten C57BL/6NHsd adult mice were either purchased from Koatech (Pyeongtaek, South Korea) or from KISAF (Korea Institute of Science and Technology, Seoul, South Korea). Mice were bred in the specific pathogen-free animal facility at KISAF (Korea Institute of Science and Technology, Seoul, South Korea) housed under a controlled 12 h light/dark cycle and temperature, with access to food and water *ad libitum*. Experiments were performed on mice at least 10 weeks old, both male and female. All procedures were approved and supervised by the Institutional Animal Care and Use Committee of Korea Institute of Science and Technology (approval No. KIST-2014-002, KIST-2019-012 and KIST-2019-099).

### Adeno associated virus preparation

Genetically encoded voltage indicators were cloned into a pAAV plasmid containing a human synapsin promoter, the woodchuck hepatitis virus post-transcriptional regulatory element, hGH poly adenylation signal, and adeno associated virus (AAV) serotype 2 inverted terminal repeat sequences.

AAVs were produced in-house according to the protocol provided by the Salk Institute viral vector core facility with modifications (Kim et al., 2015). AAVpro 293T cells (#632273, Takara Bio, Shiga, Japan) were co-transfected with a mixture of three plasmids: a pAAV plasmid, the pHelper plasmid (#6672, Takara Bio, Shiga, Japan), and the pRC1 serotype 2/1 plasmid (#6672, Takara Bio, Shiga, Japan), using the calcium phosphate transfection method. 72 h after the transfection, cells were harvested and lysed by multiple rounds of freeze-thaw and titration using a syringe and a needle, while simultaneously Benzonase nuclease (E1014, Sigma-Aldrich, Merck KGaA, Darmstadt, Germany) treated to reduce viscosity. Released AAV particles were collected via Iodixanol gradient ultracentrifugation at 183,000 g for 47 min with the NVT90 rotor (#362752, Beckman Coulter, Indianapolis, IN, United States), dialyzed in PBS with sorbitol, concentrated by centrifugal filter devices (30 KDa NMWL, Amicon Ultra-4, Merck Millipore, Cork, Ireland), and stored at  $-80^{\circ}\text{C}$  until use. Titers of the purified AAVs were estimated by performing a quantitative PCR on DNase-I treated samples, and are denoted genome content per mL (GC/mL).

### Adeno associated virus injection

Prior to injection, a glass injection pipette was pulled and fashioned from a glass capillary and then cut using a microforge to form an opening of 25–50  $\mu\text{m}$ . All transcranial injections of mice between the ages of 10–15 weeks were conducted under 1.5–3% general isoflurane anesthesia. After initial induction with anesthesia, each mouse had its head affixed to the compact mouse stereotaxic frame (MCI neuroscience, East Sussex, United Kingdom). Fur over its cranium was shorn and cleaned with 70% ethanol. Commercially available hair removal cream was used to completely remove all fur to prevent the introduction of any hair into an open incision during the injection. The naked skin was then disinfected with povidone-iodine. The cranium over the right motor cortex was exposed by a midline incision. A hole through

the cranium was made 0.9 mm rostral and  $\pm$  1.1–1.25 mm lateral from the bregma by a metal rotary tool kit (Foredom K.1070-2, Blackstone Industries, Bethel, CT, United States) with a drill bit size United States 1/4, 0.5 mm. The glass injection pipette containing an AAV was placed over the hole and lowered so that the tip of the glass pipette would be placed 0.5–0.7 mm under the surface of the primary motor cortex. 200–400 nL of the virus solution was slowly injected using the UltraMicroPump II and Micro4 controller (World Precision Instruments, Sarasota, FL, United States). After the surgery, mice were allowed to recover on a heating pad and then returned to their home cages once they were fully awake. AAV injected mice were used for the experiments 2–5 weeks after the injection.

### **Ex vivo slice preparation**

Chemicals were obtained from Sigma-Aldrich (Merck KGaA, Darmstadt, Germany) unless otherwise specified. 300  $\mu$ m thick acute coronal slices from 12–20 week old mice were prepared using a vibratome (VT-1200, Leica, Nussloch, Germany) following either sucrose artificial cerebrospinal fluid solution (aCSF) (Geiger et al., 2002; Bischofberger et al., 2006) or N-Methyl-D-glucamine (NMDG) aCSF based cutting method (Ting et al., 2014, 2018).

### **Sucrose aCSF based cutting method**

Brain is first sliced in a cold high-sucrose aCSF containing (in mM): 75 sucrose, 25 NaHCO<sub>3</sub>, 2.5 KCl, 0.5 CaCl<sub>2</sub>, 7 MgCl<sub>2</sub>, 1.25 NaH<sub>2</sub>PO<sub>4</sub>, and 25 D(+)-glucose, pH 7.4, oxygenated with a 95% O<sub>2</sub>/5% CO<sub>2</sub> gas mixture. The brain slices are then transferred to aCSF containing (in mM): 124 NaCl, 2.5 KCl, 1.25 NaH<sub>2</sub>PO<sub>4</sub>, 24 NaHCO<sub>3</sub>, 5 HEPES, 12.5 Glucose, 2 MgSO<sub>4</sub>, and 2 CaCl<sub>2</sub>, pH 7.4, oxygenated with a 95% O<sub>2</sub>/5% CO<sub>2</sub> gas mixture, and incubated for 30 min at 34°C, followed by recovery for 60 min at room temperature.

### **NMDG aCSF based cutting method**

Brain is first sliced in a cold NMDG-HEPES aCSF containing (in mM): 124 NaCl, 2.5 KCl, 1.25 NaH<sub>2</sub>PO<sub>4</sub>·2H<sub>2</sub>O, 24 NaHCO<sub>3</sub>, 5 HEPES, 12.5 Glucose, 2 MgSO<sub>4</sub>, pH 7.4, oxygenated with a 95% O<sub>2</sub>/5% CO<sub>2</sub> gas mixture. The brain slices are then incubated for 30 min at 34°C, during which NMDG aCSF with 2 M NaCl is added multiple times to bring up the NaCl concentration in a stepwise manner. The slices are then transferred to a HEPES holding aCSF containing (in mM): 92 NaCl, 2.5 KCl, 1.25 NaH<sub>2</sub>PO<sub>4</sub>, 30 NaHCO<sub>3</sub>, 20 HEPES, 25 Glucose, 5 Ascorbic acid, 2 Thiourea, 3 Pyruvate, 2 MgSO<sub>4</sub>, and 2 CaCl<sub>2</sub>, pH 7.4, oxygenated with a 95% O<sub>2</sub>/5% CO<sub>2</sub> gas mixture, and allowed to recover for 60 min at room temperature.

### **Experiment setup**

A high-speed CCD camera (Neuro CCD, RedShirt Imaging, Decatur, GA, United States) connected to the upright widefield epifluorescence microscope (Slicescope, Scientifica, East Sussex, United Kingdom) in combination with a GFP filter set (GFP3035D-OMF, Semrock, Rochester, NY, United States), LED controller (UHPLCC-01, Prizmatix, Givat-Shmuel, Israel), an ultra high power collimated LED light source (UHP-LED-460, Prizmatix, Givat-Shmuel, Israel), and a 10x water immersion objective lens

(UMPlanFL N; NA = 0.3, Olympus, Tokyo, Japan) was used for all experiments. A perfusion chamber (RC26G, Warner Instruments, Hamden, CT, United States) with a heating platform (PH-1, Warner Instruments, Hamden, CT, United States) affixed to a stage adapter (Series 20, Warner Instruments, Hamden, CT, United States) placed on a sample plate holder (Scientifica, East Sussex, United Kingdom) was used to perfuse the slices during the experiments. To record, each brain slice was placed in the recording chamber and perfused continuously with aCSF containing (in mM): 124 NaCl, 2.5 KCl, 1.25 NaH<sub>2</sub>PO<sub>4</sub>, 24 NaHCO<sub>3</sub>, 5 HEPES, 12.5 Glucose, 2 MgSO<sub>4</sub>, and 2 CaCl<sub>2</sub>, pH 7.4, oxygenated with a 95% O<sub>2</sub>/5% CO<sub>2</sub> gas mixture, at the rate of 2–3 mL/min. The recording chamber was maintained at 33°C by a temperature control unit (TC-344B, Warner Instruments, Hamden, CT, United States). For bicuculline perfused recordings, bicuculline methochloride (0131, Tocris, Bristol, United Kingdom) dissolved in aCSF at the final concentration of 20 µM was perfused over the slices.

### **Widefield epifluorescence imaging**

A time-lapse widefield epifluorescence image of the primary motor cortex was recorded using a 10x objective lens, resulting in a 500 µm × 500 µm field of view, illuminated by excitation light measuring 130 mW/mm<sup>2</sup> at the focal plane. For each acquisition, the Neuro CCD high-speed CCD camera acquired a 10,000 frame 10 s time-lapse recording of 80 × 80 pixels at 1 kHz.

### **Quick analysis during a recording session**

Ten second time-lapse widefield epifluorescence recording of the 6,400 pixels was immediately processed after acquisition using the NeuroPlex software (RedShirt Imaging, Decatur, GA, United States). The time-lapse fluorescence signals of all the pixels within the region of interest roughly encompassing the brightest area were spatially averaged. The spatially averaged time-lapse fluorescence signal was bandpass filtered between 5 and 50 Hz using the 5th order Butterworth high-pass and low-pass filters and converted to fractional fluorescence change values using appropriate reference frames,  $\Delta F/F_{ref} = (F - F_{ref}) / F_{ref}$ . This quick on-the-spot analysis allowed us to determine the success of each 10 s recording during a 6 h recording session.

### **Movies**

Movies of the oscillations in MPEG format were created by taking 50-100 frames prior to the onset of an oscillation to 50-100 frames after cessation of an oscillation. Each 80x80 pixel frame was spatially low pass filtered using a mean filter with a 3x3 pixel kernel, and the maximum and minimum of the intensity range was automatically set to maximize the dynamic range of the movie without saturating any of the pixels, and pseudocolored to better visualize the changes in fluorescence intensity. All movies were slowed down 33fold from their 1 kHz acquisition frequency to play back at 30 frames per second or 30 Hz.

### **Representative oscillation of a recording**

For each observed oscillation, an unmasked pixel whose oscillation waveform had the largest %  $\Delta F/F_0$  was chosen as the reference pixel. To come up with a representative



oscillation of a recording, pixels displaying oscillation waveforms highly correlated to the reference pixel were selected in such a way that addition of any of the remaining correlated pixels will significantly worsen the signal-to-noise ratio of the averaged oscillation waveform. The number of pixels chosen varied from 142 to 1,583, with a median of 629 pixels. The time at which the representative oscillation waveform gets larger than  $3\sigma$  or smaller than  $3\sigma$  of the Gaussian baseline noise is considered to be the starting point and end time point of the representative oscillation waveform, respectively.

### Data analysis

Data analysis was carried out offline using MATLAB scripts (MATLAB R2021b; The MathWorks, Natick, MA, United States).

### Pre-processing

Data pre-processing included photobleaching artifact removal, temporal band-pass filtering within [1, 50] Hz based on the 3rd order Butterworth filter (applied in zero-phase mode) and the baseline z-normalization of the recorded signals. The latter was applied, independently, to the trace associated with each pixel by using the corresponding mean and standard deviation of signal values from the pre-oscillation interval (-8, -0.5) s. According to this normalization, negative z-scores correspond to depolarization whereas positive ones to hyperpolarization. Baseline z-score normalization is a popular method for time normalization, suitable for the functional organization measurements we performed in our analysis. Compared to the conventional  $\Delta F/F_0$  approach, z-score normalization avoids the temporal correlation among traces associated with different pixels around the reference frame. The aforementioned treatment gave rise to the multisite optical signal (or video sequence), based on which our analysis was carried out:

$$\chi_{n,m}(t), n, m = 1, 2, \dots, 80 \quad t = 1, 2, \dots, 10,000$$

In the adopted notation, the pair  $(n, m)$  corresponds to the coordinates of a particular pixel on the imaged plane,  $t$  indicates the discrete time, whereas  $fs$ , the sampling frequency, had been set to 1kHz.

### Reconstructing and characterizing the functional network across several recording conditions

In this algorithmic pipeline, that was carried based on single-trial response data, the input was the ensemble of pixel traces  $\{x_i(t)\}_{i=1, 2, \dots, 6400}$ , without any direct reference to their spatial coordinates. Using the Spearman's rank correlation coefficient  $\rho_{ij} = \rho(x_i(t), x_j(t))$ , the functional covariation was quantified between every possible pair of recording sites. The related measurements were rectified, i.e.,  $r_{ij} = \text{abs}(\rho_{ij})$ , and tabulated in a symmetric rectangular matrix  $\mathbf{R}_{[6400 \times 6400]}$ , that was treated as the matrix representation of a complex network, namely the (reconstructed) functional network. The procedure was repeated using equitemporal (10 s) segments from three distinct recording conditions: bicuculline-treated, but no observed ripples  $\mathbf{W}=\mathbf{R}^{no}$ ; bicuculline-treated, before observing ripples  $\mathbf{W}=\mathbf{R}^{bef}$ ; bicuculline-treated, observed

ripples  $W=R^{\tau p}$ . For any trial-dependent and condition-dependent instantiation,  $W$  was considered as the connectivity pattern of a graph with nodes that were associated to pixels and a structure that was reflecting the functional organization of the imaged slice. Altering the level of edge density resulted in qualitatively similar conclusions regarding the reported comparisons; therefore, a sparsification step was employed by zeroing the entries in  $W$  that corresponded to 50% of weakest connections. Finally, based on the sparse connectivity pattern  $W^*$ , three network metrics were derived, namely *Strength*, *Global* and *Local Efficiency*, all in reference to individual nodes.

In the context of network science, the *Strength* of a node refers to a quantitative measure of the importance or influence of that node within the network. In our case, it was defined as the degree centrality of that node, i.e., the number of edges that are connected to it:

$$S_i = \sum_{j \neq i} w_{ji}^*$$

The *Global Efficiency* (GE) of a node is a measure of the efficiency of communication in the network when that node is removed and can be thought of as the most efficient route between two nodes, in terms of the number of edges that must be traversed. It is directly linked with the concept of shortest paths, i.e., it is calculated as the average inverse shortest path length between all pairs of nodes in the network when the node in question is removed. In our case, the shortest path between a pair of nodes was estimated after turning the functional coupling strengths to pairwise distances, i.e.,  $d_{ji} = 1 - w_{ji}^*$ , and applying Dijkstra's algorithm. Adopting the formulation in (Fornito et al., 2016), the global efficiency of a node was defined as:

$$GE_i = \frac{1}{(N_{pixels} - 1)} \sum_{j \neq i} \frac{1}{l_{ij}}$$

with  $l_{ij}$  denoting the length of shortest path between nodes (i.e., pixels)  $i$  and  $j$ .

The *Local Efficiency* (LE) of a node is a measure of the resilience of a network to the removal of that node and can be thought of as a measure of the efficiency of communication between the immediate neighbors of a node if that node were to be removed. In our case, it was estimated by first restricting the above computations to each subgraph  $G_i$ , containing the neighbors of a node  $i$ , and then integrating across the nodes in the subgraph:

$$LE_i = \frac{1}{N_{G_i}(N_{G_i} - 1)} \sum_{r, k \in G_i} \frac{1}{l_{rk}}$$

## Results

### ArLight successfully detects spontaneous oscillatory activity

*Ex vivo* application of 40  $\mu$ M bicuculline to block GABA<sub>A</sub> receptors in the motor cortex slices expressing ArLight (Jin et al., 2012; Han et al., 2014) under the control of human

synapsin 1 (hSyn) promoter, resulted in spontaneous widespread oscillatory activity in the upper layers of the motor cortex (Altamura et al., 2006) observable with the widefield fluorescence microscopy (Fig. 1). A stereotypical oscillation showed a large initial deflection, either depolarizing or hyperpolarizing, followed immediately by 2-19 fluctuations that typically decreased in amplitude over time (Fig. 1C). Although all observed oscillations followed the stereotypical pattern, there was considerable heterogeneity in the representative oscillation waveforms observed among all slices (Fig. 1C). In addition, considering that, unlike electrophysiological recordings fluorescent GEVI imaging preserves the spatial information about the neural activity,

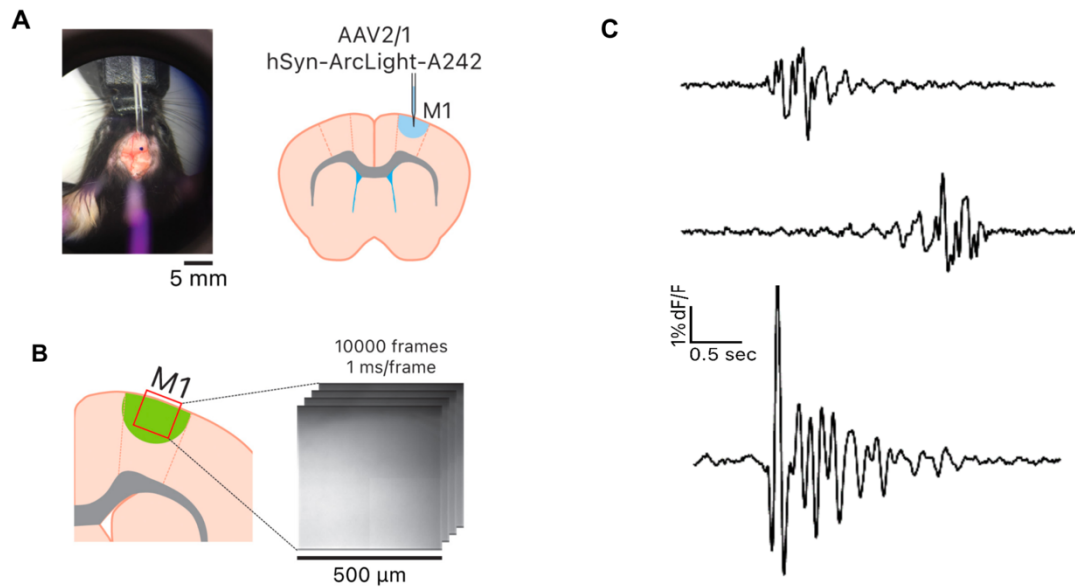


**Figure 1.** Observation of the oscillations in the motor cortex. **(A)** View of stereotaxic dissection scope over the area of AAV injection and the injection location in the primary motor cortex. **(B)** Imaging location in the primary motor cortex. **(C)** Representative oscillation waveform for three recordings from two different slices.

creating and comparing time-lapse fluorescent movies of the oscillations revealed that spatial neural activity similarly also displayed heterogeneity. More specifically, eight out of 19 oscillations displayed a spatially limited fluctuation in fluorescence, whereas 11 out of 19 oscillations displayed a widespread (whole slice) oscillation.

### **Ripple anticipation does not imply a network shift in terms of information transfer efficiency**

At the first stage of our analysis, we sought to characterize the emerged network and identify any discernible patterns in the functional network that could serve as a reliable predictor for future oscillatory events, and thereby shed light on the underlying network dynamics that give rise to these phenomena in terms of information transfer. To this end, three well-known metrics were estimated and compared between two recording conditions (Fig. 2; Fig. S1): a baseline network state, corresponding to recordings where application of bicuculline did not result in future oscillatory behavior (bicuculline-treated, no observed ripples;  $W=R^{no}$ ) and an intermediate state aiming to capture any gradual shifts in network dynamics leading up to the onset of oscillations (bicuculline-treated, before observing ripples;  $W=R^{bef}$ ).

The results were first derived at the level of individual nodes (i.e., pixels) and then averaged so as to be suggestive of the overall observed connectivity network (i.e., whole slice). The metric of strength, here, serves as a *centrality* measure and indicates the average importance of each node within the observed connectivity network. GE reflects the average importance of each node in the information transfer within the overall network, whereas LE reflects the average importance of each node within the local network it belongs to.

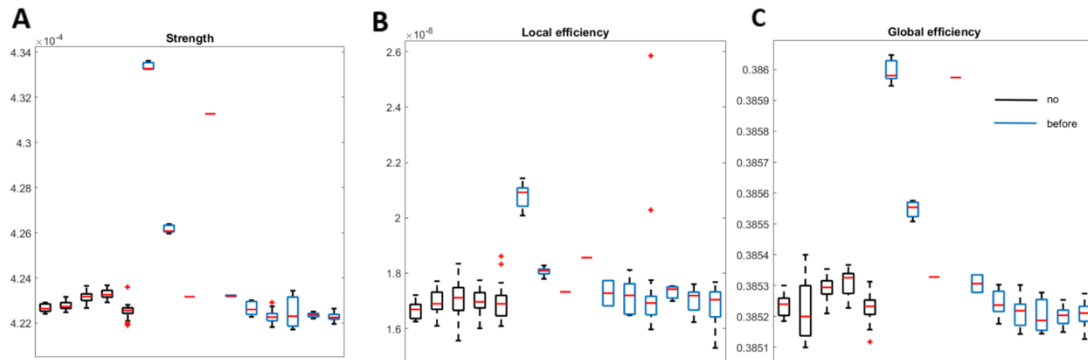


**Figure 2.** Contrastive representation (bicuculline-treated, no observed ripples vs. bicuculline-treated, before observing ripples) at the level of individual slices (5 vs. 10). From left to right: Strength, Local Efficiency and Global Efficiency at the level of individual slices, averaged across pixels. On each box, the central (red) mark indicates the median, and the bottom and top edges of the box indicate the 25th and 75th percentile, respectively. The whiskers extend to the most extreme data points not considered outliers, and the outliers are plotted individually using the "+" symbol. Regarding the bicuculline-treated, before observing ripples case, individual red marks without a box denote that for this specific slice only a single recording was available. All compared distributions were statistically different, based on Wilcoxon ranksum test, at confidence level of  $\alpha = 0.01$ .

Preliminary results indicated a quantitative difference between the two recording conditions: for the second condition (i.e., bicuculline-treated, before observing ripples), the three network measures averaged over the imaged plane moved to larger values (Fig. 2; first two blue boxes), whereas the probability distribution of the correlation weight strengths moved to larger values as well, with virtually zero inter-trial variability hinting a network shift towards a more efficient regime of information transfer, as it was slowly approaching the threshold for oscillatory behavior. Thus, a plausible hypothesis emerged, namely that as the network progresses slowly from an equilibrium towards an oscillatory state, a detectable increase in the network metrics could, in principle, be apparent. However, this remark failed to generalize as more experiments were conducted (Fig 2; rest boxes), hinting at the insufficiency of a network theory perspective to provide us with a reliable anticipatory predictor of future spontaneous oscillatory events.

### **Approaching oscillatory behavior is not linked to a traceable network function reorganization**

Given that the size of the  $W=R^{bef}$  condition (i.e., the total number of available trial recordings for this condition) was totally dependent on whether the first ripple event occurred early or late in the recording session, we next estimated and compared the aforementioned network metrics between the last trial recording from the  $W=R^{bef}$

condition and the first trial recording from the  $W=R^{TP}$  condition (Fig. 3A), under the hypothesis that since spontaneous synchronized discharges can occur even in isolated blocks of the neocortex, mechanisms for initiating this activity must reside within the cortex itself and this should, in principle, be translated to a notable change in the system's function organization, reflecting a shift in its efficiency. However, the under-

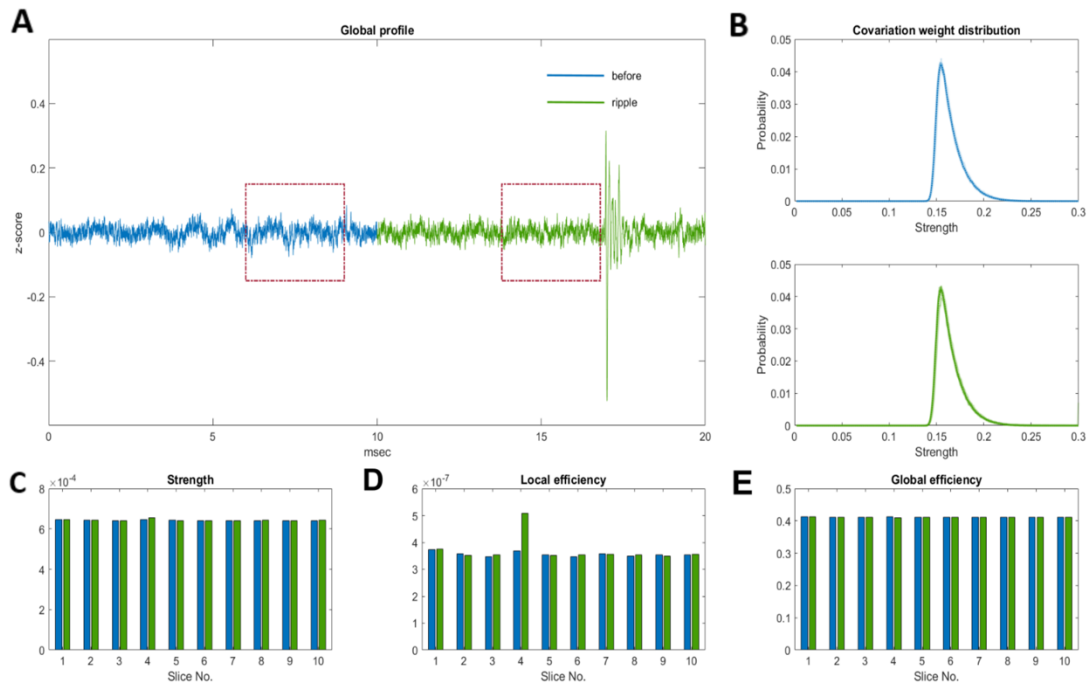


**Figure 3.** Contrastive representation (last trial recording of the bicuculline-treated, before observing condition vs. first trial of the bicuculline-treated, observer ripples condition). **(A)** Indicative example showing the temporal continuity between the two conditions. In both cases, a window of length 1,500 ms was used (dashed red box) for the reconstruction of the functional network. **(B)** Probability distribution of the correlation weight strengths, **(C)** Strength, **(D)** Local Efficiency and **(E)** Global Efficiency, averaged across pixels. All compared distributions were statistically different, based on Wilcoxon ranksum test, at confidence level of  $\alpha = 0.01$ .

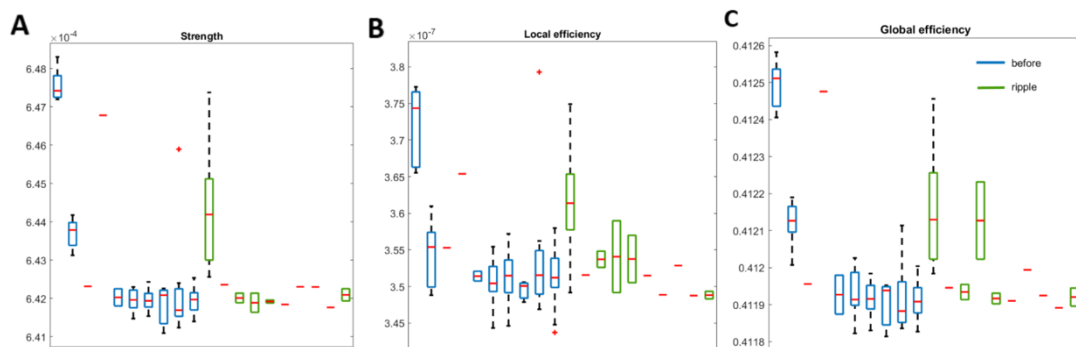


**Figure 4.** Contrastive representation (bicuculline-treated, before observing ripples vs. bicuculline-treated, observed ripples) at the level of individual slices (10 vs. 10). From left to right: Strength, Local Efficiency and Global Efficiency at the level of individual slices, averaged across pixels. On each box, the central (red) mark indicates the median, and the bottom and top edges of the box indicate the 25th and 75th percentile, respectively. The whiskers extend to the most extreme data points not considered outliers, and the outliers are plotted individually using the "+" symbol. For both conditions, individual

red marks without a box denote that for this specific slice only a single recording was available. All compared distributions were statistically different, based on Wilcoxon ranksum test, at confidence level of  $\alpha = 0.01$ .

lying communication pattern appeared to unfold in almost an identical way in both conditions. The networks exhibited weight strength distributions with similar profiles and values and reproducibility (Fig. 3B); also, no specific pattern emerged in any of the three metrics (Fig. 3C-E).

### **Moving away from a ripple does not imply a network shift in terms of information transfer efficiency**

At the final stage of our analysis, we examined the inverse case of returning to the baseline after a ripple event has occurred, under the hypothesis that such a rebound cannot take place instantaneously and this should, in principle, be reflected to a shift in network's efficiency compared to the baseline condition  $W=R^{bef}$ . As seen in (Fig. 4), for all three network measures, but especially for the case of local and global efficiencies, the results for the  $W=R^{rp}$  condition exhibit, on average, a wider distribution of values, but not necessarily a quantitative increase. Although such dispersion in the data is partially expected, due to ArcLight's sensitivity, no safe conclusion could be drawn regarding the emerged networks between the two recording conditions.

## **Discussion**

Here, using ArcLight, currently the most reliable GEVI in the hands of the experimenter (Rhee et al., 2021), we imaged and optically reported neuronal circuit activity from a population of cells in the brain slice of motor cortex *ex vivo*. We were able to detect spontaneous ensemble firing of the neurons resulting in an oscillation in the motor cortex using wide-field epifluorescence microscopy. Therefore, ArcLight-based GEVIs, with its unprecedented spatiotemporal detail, can be considered as a powerful alternative to calcium imaging or even the use of voltage sensitive dyes to image neural activity, although, clearly, faster and brighter GEVIs with larger dynamical range will eventually become available.

The primary objective of this thesis was to investigate the benefits of combining ArcLight with a network theory perspective in studying the dynamics of neural circuits during spontaneous oscillatory behavior and perhaps, identifying patterns in the functional network that could predict upcoming ripple events. More specifically, our analysis consisted of describing and quantifying information exchange among recording sites through the prism of network science (Fornito et al., 2016; Varley and Sporns, 2022; Sporns, 2022); an approach that has been successfully applied in previous studies of neural dynamics at different scales and species (Zuo et al., 2012; Johnson et al., 2018; Nakajima et al., 2021; Seguin et al., 2023). Working in purely exploratory mode, we sought to identify any discernible patterns in the functional networks between three separate recording conditions that could serve as reliable predictors of oscillatory behavior.

Although preliminary results indicated clearly that ripple anticipation is associated with increased coordination in the network, such hypothesis failed to generalize as more experiments were conducted. This could reflect either the insufficiency of the

method or unaccountable experimental uncertainties, as the experiments took place at different times during a timespan of 2 years. However, the absence of a traceable network reorganization at times surrounding a ripple event, as evident in the remarkable invariance of the underlying communication pattern, seem to suggest that, despite it could reflect the shortcoming of currently available GEVIs in meeting experimental demands, such ineffectiveness is most likely due to the limitation of a network theory perspective in being used as a data exploratory tool in spontaneous settings.

While certain technical limitations regarding GEVIs persist (Nakajima et al., 2021; Rhee et al., 2022), the ability to analyze specific cell-type behavior enhances our understanding and stimulates the emergence of new avenues of investigation. In addition, the ability to analyze such large datasets of voltage fluctuations resolved in space, time and cell types in a systematic way is of great importance. While a network theory perspective offers such a powerful framework, the results presented both here and in (Antoniadis, 2019) seem to suggest that, perhaps, in order to understand, alternative interdisciplinary intuitions about the functional meaning of the data should be considered.

## **Acknowledgments**

This work was supported by grants from the Hellenic Foundation for Research and Innovation (HFRI-FM17-286) and the Korea Institute of Science and Technology (KIST-2E30963). The author thanks Efstratios Kosmidis for valuable guidance and feedback on the manuscript, Jun Kyu Rhee, Bradley Baker and Efstratios Kosmidis for carrying out the experiments, and Nikolaos Laskaris for helpful discussions and feedback during this project.

## **References**

- Altamura, C. et al. (2006). Altered neocortical cell density and layer thickness in serotonin transporter knockout mice: a quantitation study. *Cereb. Cortex*, 17, pp. 1394-1401.
- Antoniadis, S. (2019). Analyzing spontaneous activity and network organization in transgenic mouse hippocampal area CA1 via optical recordings. Diploma Thesis.
- Averbeck, B.B. and Lee, D. (2004). Coding and transmission of information by neural ensembles. *Trends Neurosci.*, 27(4), pp. 225-230.
- Bando, Y. et al. (2019). Genetic voltage indicators. *BMC Biol*, 17(1)
- Bando, Y., Sakamoto, M., et al. (2019). Comparative evaluation of genetically encoded voltage indicators. *Cell Rep*, 26(3), pp. 802-813.e4.
- Bassett, D.S. and Sporns, O. (2017). Network neuroscience. *Nat. Neurosci.*, 20(3), pp. 353-364.
- Betz, R.F. (2022). Network neuroscience and the connectomics revolution. *Connectomic Deep Brain Stimulation*, pp. 25-58, Elsevier.
- Bullmore, E. and Sporns, O. (2009). Complex brain networks: graph theoretical analysis of structural and functional systems. *Nat. Rev. Neurosci.*, 10(3), pp. 186-198.

- Buzsáki, G. (2006). *Rhythms of the brain*. Oxford University Press, Oxford, New York.
- Buzsáki, G. and Watson, B.O. (2012). Brain rhythms and neural syntax: implications for efficient coding of cognitive content and neuropsychiatric disease. *Dialogues Clin. Neurosci*, 14(4), pp. 345-367.
- Cabral, J. et al. (2022). Metastable oscillatory modes emerge from synchronization in the brain spacetime connectome. *Commun. Phys*. 5(184).
- Carrillo-Reid, L. et al. (2017). Imaging and optically manipulating neuronal ensembles. *Ann. Rev. Biophys*, 46(1), pp. 271-293.
- Churchland, P.S. and Sejnowski, T.J. (1992). *The computational brain*. MIT Press.
- Di Volo, M. and Destexhe, A. (2021). Optimal responsiveness and information flow in networks of heterogeneous neurons. *Sci. Rep.*, 11(1).
- Dong, C. et al. (2022). Fluorescence imaging of neural activity, neurochemical dynamics, and drug-specific receptor conformation with genetically encoded sensors. *Annu. Rev. Neurosci.*, 45(1), pp. 273-294.
- Fröhlich, F. (2015). Experiments and models of cortical oscillations as a target for noninvasive brain stimulation. *Prog. Brain. Res.*, 222(3), pp. 41-73.
- Fornito, A. et al. (2016). *Fundamentals of brain network analysis*. Academic Press.
- Grienberger, C. and Konnerth, A. (2012). Imaging calcium in neurons. *Neuron*, 73(5), pp. 862-885.
- Han, Z. et al. (2014). Mechanistic studies of the genetically encoded fluorescent protein voltage probe arLight. *PLoS One*, 9(11). p. e113873.
- Hirschmann, J.V. et al. (2022). Neuronal oscillation predict deep brain stimulation outcome in Parkinson's disease. *Brain Stimulation*, 15(3), pp. 792-802.
- Hopfield, J.J. (1982). Neural networks and physical systems with emergent collective computational abilities. *PNAS*, 79(8), pp. 2554-2558.
- Izhikevich, E.M. (2010). *Dynamical systems in neuroscience: the geometry of excitability and bursting*. MIT Press.
- Johnson, G. A., et al. (2018). Whole mouse brain connectomics. *J. Comp. Neurol.*, 527(13), pp. 2146-2157.
- Jin, L. et al. (2012). Single action potentials and subthreshold electrical events imaged in neurons with a fluorescent protein voltage probe. *Neuron*, 75(5), pp. 779-785.
- Leckman, J.F. et al. (2006). Tourette syndrome: a relentless drumbeat - driven by misguided brain oscillations. *J. Child Psychol. Psychiatry*, 47(6), pp. 537-550.
- Lee, S. et al. (2016). Imaging membrane potential with two types of genetically encoded fluorescent voltage sensors. *J. Vis. Exp.*, 4:e53566.



- Mably, A.J. and Colgin, L.L. (2018). Gamma oscillations in cognitive disorders. *Curr. Opin. Neurobiol.*, 52, pp. 182-187.
- Mank, M. and Griesbeck, O. (2008). Genetically encoded calcium indicators. *Chem. Rev.*, 108(5), pp. 1550-1564.
- Mendes, R.A.V. et al. (2021). Hijacking of hippocampal-cortical oscillatory coupling during sleep in temporal lobe epilepsy. *Epilepsy Behav.*, 121, p. 106608.
- Nadeau, S.E. (2020). Neural population dynamics and cognitive function. *Front. Hum. Neurosci.*, 14.
- Nakajima, R., et al. (2016). Optogenetic monitoring of synaptic activity with genetically encoded voltage indicators. *Front. Synaptic Neurosci.*, 8.
- Nakajima, R. et al. (2021). GEVI cell-type specific labelling and a manifold learning approach provide evidence for lateral inhibition at the population level in the mouse hippocampal CA1 area. *Eur. J. Neurosci*, 53(9), pp. 3019-3038.
- Neige, C., Yadav, G. and Derosiere, G. (2023). The oscillatory nature of movement initiation. *J. Neurosci.*, 43(6), pp. 882-884.
- Piatkevich, K. D. et al. (2018). A robotic multidimensional directed evolution approach applied to fluorescent voltage reporters. *Nat. Chem. Biol.*, 14(4), pp. 352-360.
- Pikovsky, A., Rosenblum, M., Kurths, J. (2001). *Synchronization: a universal concept in nonlinear sciences*. Cambridge University Press.
- Platisa, J. et al. (2022). Voltage imaging in the olfactory bulb using transgenic mouse lines expressing the genetically encoded voltage indicator arclight. *Sci. Rep.*, 12(1).
- Rhee, J.K. et al. (2020). Biophysical parameters of GEVIs: considerations for imaging voltage. *Biophys. J.*, 119(1), pp. 1-8.
- Rhee, J.K., Iwamoto, Y. and Baker, B.J. (2021). Visualizing oscillations in brain slices with genetically encoded voltage indicators. *Front. Neuroanat.*, 15.
- Seguin, C. et al. (2023). Communication dynamics in the human connectome shape the cortex-wide propagation of direct electrical stimulation. *Neuron*, 111(9), pp. 1391-1401.e5.
- Singh, A.D. (2018). Oscillatory activity in the cortico-basal ganglia-thalamic neural circuits in Parkinson's disease. *Eur. J. Neurosci.*, 48(8), pp. 2869-2878.
- Sporns, O. (2018). Graph theory methods: applications in brain networks. *Dialogues Clin. Neurosci.*, 20(2), pp. 111-121.
- Sporns, O. (2022). The complex brain: connectivity, dynamics, information. *Trends Cogn. Sci.*, 26(12), pp. 1066-1067.
- Valley, T.F. and Sporns, O. (2022) Network analysis of time series: novel approaches to network neuroscience. *Front. Neurosci.*, 15.

Wallis, J.D. (2018). Decoding cognitive processes from neural ensembles. Trends Cogn. Sci., 22(12), pp. 1091-1102.

Wang, X.J. (2010). Neurophysiological and computational principles of cortical rhythms in cognition. Physiol. Rev., 90(3), pp. 1195-1268.

Xu, Y., Zou, P. and Cohen, A.F. (2017). Voltage imaging with genetically encoded indicators. Curr. Opin. Chem. Biol., 39, pp. 1-10.

Yang, H. and St-Pierre, F. (2016) . Genetically encoded voltage indicators: opportunities and challenges. J. Neurosci., 36(39), pp. 9977-9989.

Yuste, R. (2015). From the neuron doctrine to neural networks. Nature Rev. Neurosci, 16(8), pp. 487-497.

Zuo, X.-N. et al. (2012). Network centrality in the human functional connectome. Cereb. Cortex, 22(8), pp. 1862-1875.

## Supplementary material

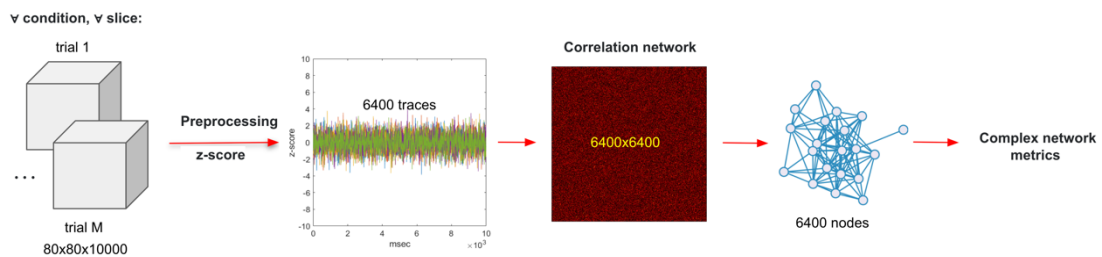


**Figure S1.** Algorithmic pipeline for reconstructing and characterizing the functional network.

## RESEARCH PROPOSAL

### Title

Mapping and monitoring the effects of striatal inhibition on motor cortex using transgenic mouse lines expressing the genetically encoded voltage indicator ArcLight

### Project summary

Deep brain stimulation (DBS), a neurosurgical procedure that involves the implantation of electrodes in targeted brain regions, typically the basal ganglia, to deliver precisely controlled electrical stimulation has demonstrated efficacy in mitigating motor symptoms associated with various neurological disorders. However, its precise therapeutic mechanisms still remain poorly understood. Building on the recent advances in the development of both potent genetically encoded voltage indicators (GEVIs), chimeric proteins that allow optical recordings of membrane potential changes in defined cell populations, and transgenic reporter animals that facilitate precise and repeatable targeting with high expression levels, this project aims to contribute towards a better understanding of the various mechanisms underlying DBS by establishing a solid foundation for *in vivo* monitoring and assessment of its effects on the corresponding motor cortex output response. To this end, we will develop and apply transgenic mouse lines expressing the GEVI ArcLight in order to optically record the neuronal electrical activity of different cell types in the motor cortex *in vivo*, following striatal disinhibition. Complementary to this, advanced data analysis techniques will be employed in order to characterize and study the neurophysiological consequences of the emerging functional network. The outcomes of this research have the potential to shape future DBS studies and therefore lead to improved clinical outcomes.

### Project description

#### *Specific aims*

This project aims to set a foundation for monitoring the effects of DBS in the basal ganglia on the corresponding motor cortex output response *in vivo*. We propose to express ArcLight, a potent GEVI for *in vitro* and *in vivo* imaging, in the motor cortex of transgenic mouse lines targeting either calcium/calmodulin-dependent protein kinase type II alpha chain-positive (CaMKII $\alpha$ +) pyramidal cells or parvalbumin-positive (PV+) inhibitory interneurons in respective *cre-lox* strains to image their activity *in vivo* in single trials using widefield epifluorescence imaging, following the acute disinhibition of the GABA<sub>A</sub>R inhibitory circuit in the dorsal sensorimotor putamen with bicuculline. Bicuculline-induced responses and rest state activity of CaMKII $\alpha$ + and PV+ populations will be recorded using fast optical recordings (>1kHz) to explore whether such disinhibition will eventually give rise to spontaneous oscillatory activity in the motor cortex *in vivo* and if so, whether or not we can derive any meaningful insight into each specific cell type's role in generating these oscillations. To this end, data

analysis techniques based on the principles of data-manifold learning and graph-theory, that enable the intelligible synopsis of stimulus-induced phenomena in optical imaging data will be used to study the evolving dynamic relationships and reveal the functional connectome of the network. With the aforementioned arsenal of tools, we will attempt to address the following objectives:

**Objective 1:** Report the first *in vivo* experiments using transgenic mouse lines as vehicles for expression of the GEVI ArcLight in the motor cortex

**Objective 2:** Determine the effect of striatal inhibition in shaping and determining the spatiotemporal output response of the motor cortex

**Objective 3:** Study the role of different functional classes of motor cortex neurons in generating oscillations.

### ***Introduction and significance***

Historically arising from functional stereotactic neurosurgery techniques used to produce selective lesions of specific deep brain structures (thalamic and cerebellar nuclei), DBS has emerged over the years as a treatment for Parkinson's disease, dystonia, epilepsy, cluster headache, memory loss, obsessive-compulsive disorder, Tourette syndrome, as well as depression (Benabid et al., 1987, 2009; Lozano & Hamani, 2004; Bernstein & Peters, 2005; Delaloye & Holtzheimer, 2014; Baumgartner et al., 2022; Malvea et al., 2022; Liu et al., 2022). Despite its nearly three-decade history, though, the underlying mechanisms by which DBS effectively ameliorates such a wide range of neurological disorders still lack comprehensive understanding. Having an optical readout of activity from different components of neuronal circuits affected by DBS is crucial, particularly in conditions such as Parkinson's disease and Tourette syndrome, as this would enable monitoring the disrupted balance between excitation and inhibition, and thus help explain the therapeutic mechanism leading to improved clinical outcomes.

The development of potent GEVIs over the last few years provides the opportunity for such monitoring to become possible (Jin et al., 2012; Han et al., 2014; Lee et al., 2016; Nakajima et al., 2016; Baker et al., 2017). Since voltage indicators are a direct measurement of changes in membrane potential, the time has come for them to be tested as a powerful monitoring tool which could potentially detect the effects of DBS on restoring the balance between neuronal activation and inhibition. Despite certain limitations, such as a lower signal-to-noise ratio than their counterparts, calcium indicators, GEVIs continue to improve both in the size of the optical signal as well as in the speed of the response. Recent comparisons of different GEVIs demonstrated that ArcLight-based GEVIs gave the most consistent signal and were able to successfully report network activity for widefield epifluorescence recordings both *in vivo* and *ex vivo* (Borden et al., 2017; Bando et al., 2019; Milosevic et al., 2020; Rhee et al., 2021, Platasa et al., 2022). In addition, the development of novel transgenic mouse lines that facilitate precise and repeatable targeting with high expression levels and signal-to-noise ratio suggest that the time is ripe for applying such mouse lines as vehicles for GEVI expression in studies of the *in vivo* mammalian brain, and therefore overcome limitations associated with current mammalian *in vivo* approaches such as

in utero electroporation or injection of a viral vector (Madisen et al., 2015; Daigle et al., 2018; Song et al., 2018; Shimaoka et al., 2019; Platisa et al., 2022).

Selective disruption of the basal ganglia output in non-human primates by administering the GABA<sub>A</sub>R receptor antagonist bicuculline to focally disinhibit the dorsal sensorimotor putamen results in facial and somatic motor tics resembling those observed in human Tourette syndrome patients (McCairn et al., 2009, 2016; Worbe et al., 2009, 2013). Additionally, local field potential recordings along the cortico-basal-ganglia-thalamo-cortical loop, captured during motor tic events in both non-human primates and human patients reveal distinctive neural patterns characterized by an abrupt spike followed by oscillations phase coupled in the alpha frequency range (7-14 Hz) in the thalamus, basal ganglia, anterior cingulate cortex, as well the primary motor cortex (McCairn et al., 2009; Marceglia et al., 2017). These results suggest that the acute disinhibition of GABA<sub>A</sub>R inhibitory circuit in the dorsal sensorimotor putamen gives rise to oscillatory activity in the thalamus and basal ganglia, which subsequently propagates ipsilaterally through the anterior cingulate to the motor cortex.

Following earlier *in vivo* and *ex vivo* experiments in the rat primary motor cortex (Castro-Alamancos, 2000; Rhee et al., 2021; Antoniadis, 2023) which showed that directly disinhibiting the GABA<sub>A</sub>R inhibitory network results in recorded large amplitude oscillations and the recent success of using the GEVI ArcLight to optically record the neuronal electrical activity of different cell types *in vivo* (Platisa et al., 2022), this project endeavors to lay the groundwork for a fundamental experimental framework upon which future studies aiming to unveil the therapeutic mechanism of DBS may rely.

### **Research strategy**

The project is organized around 4 work packages concerning *in vivo* rest state activity recordings following generation of two de novo mouse lines with distinct patterns of ArcLight expression in the motor cortex, *in vivo* recordings upon acute striatal GABA<sub>A</sub>R disinhibition via bicuculline microinjection, data analysis to functionally characterize different aspects of motor cortex physiology, and results dissemination. To ensure smooth deployment of the project, one post-doctoral fellow with documented experience in *in vivo* mammalian brain studies focusing on motor cortex neurophysiology, as well as a graduate student experienced in big data analytics and machine learning, will be recruited. At least two publications are anticipated in high-profile neuroscience journals, one on voltage imaging in the motor cortex using transgenic mouse lines expressing ArcLight and one on the effects of striatal inhibition on motor cortex output and what it entails for future DBS studies. All data-related activities will be supervised for the whole duration of the project to ensure that its activities are in-line with the EU regulations in terms of ethical, legal and privacy practices. Efforts will be made to make all results and the analysis code as open to the scientific community as possible. The duration of this project is 36 months.

### **Work Package 1: In vivo rest activity recordings in the motor cortex**

**Objectives:** Generate two novel mouse lines with distinct patterns of ArcLight expression in different cell types of the motor cortex. Reveal aspects of self-organization principles in the cortical network dynamics. Characterize the response of CaMKII $\alpha$ + and PV+ neurons.

**Description:** The overall aim of this work package is the generation of two transgenic mouse lines in which the GEVI ArcLight will be targeted to two different cell populations and, consequently, to verify whether it is indeed able to optically report neuronal circuit activity *in vivo* in order to examine different aspects of motor cortex physiology. To this end, we will take advantage of a novel transgenic reporter mouse, Ai86 (TITL-ArcLight) (JAX Stock #034694) to selectively drive the expression of the GEVI ArcLight in CaMKII $\alpha$ + neurons and PV+ interneurons of the motor cortex. Ai86 is a Cre/tTA double reporter mouse line in which the GEVI ArcLight A242 is knocked into the TIGRE locus (TIGRE 1.0) (Madisen et al., 2015; Daigle et al., 2018). For this project, the Ai86(TITL-ArcLight) founder line will be independently crossed to either Camk2a-tTA (JAX Stock #007004) or Pv-Cre (JAX Stock #008069) to yield double mutant lines Ai86 x Camk2a-tTA and Ai86 x Pv-Cre, respectively. The transgenic offspring of these lines will be crossed to create a triple transgenic mouse line Ai86 x Camk2a-tTA x Pv-Cre with ArcLight expression targeted to PV+ GABAergic interneurons in the motor cortex. A second triple transgenic line with ArcLight targeted to CaMKII $\alpha$ + pyramidal cells in layer II and III will also be created by crossing Ai86 x Camk2a-tTA and Camk2a-Cre (JAX Stock #005359) lines. We will confirm the presence of ArcLight, tTA, and Cre using PCR-based genotyping on all experimental animals. Mice will be housed under standard environmental conditions, with room temperature ranging between 23-25 degrees Celsius under a 12h light/dark cycle and measurements will be made during the light phase.

Our functional image experiments will be carried out in male and female mice aged between 30-180 days. Ketamine/xylazine, an antagonist for NMDA receptors, will be used to induce and maintain a deep anesthetic state via intraperitoneal injections as in (Platisa et al., 2022). Additional comparisons between awake and anesthetized states may be conducted, as inducing anesthesia is known to introduce confounding variables that influence experimental measurements. Throughout the procedure the body temperature will be maintained at 37 degrees Celsius. The skin above the cranium and motor cortex will be removed, and a custom head-post will be fixed to the back of the skull. The mouse will then be mounted on a custom-made holder, allowing for precise head positioning and fixation.

In order to study the fluctuating, self-regulated, integration/segregation tendencies observed in the neuronal activity of the motor cortex, we will use a high-speed CMOS camera connected to the c-mount of an upright epifluorescence microscope in combination with a GFP filter set and a 10x dry or a 20x water immersion objective lens. 8.8 mW of light will be applied through the conventional epi-light source port to illuminate the whole field of view (1.7 mm diameter, 3.7 mW/ mm<sup>2</sup>). The fluorescent signal of ArcLight will be acquired at 128 x 128 pixels, 1 kHz sampling rate from primary motor cortex (500  $\mu$ m x 500  $\mu$ m) by the CMOS camera using the NeuroPlex software (RedShirt Imaging, Decatur, GA, United States). Recordings will last for 10 sec (10,000

frames). For data analysis, averages of 10 trials with 10 sec intervals will be used, unless otherwise required.

### **Work Package 2:** In vivo recordings upon acute striatal GABA<sub>A</sub>R disinhibition

**Objectives:** Determine the effect of striatal inhibition in shaping and determining the spatiotemporal output response of the motor cortex. Study the role of different functional classes of motor cortex neurons in generating oscillations.

**Description:** The next important question to be answered is how striatal inhibition shapes and determines the motor cortex network's response. The aim here will be to contrast control recordings with recordings following pharmacological blockage of GABAergic synapses in the dorsal sensorimotor putamen for both cell-type populations. Following earlier conclusions (McCairn et al., 2009; Marceglia et al., 2017), we predict that the acute disinhibition of GABA<sub>A</sub>R inhibitory circuit in the striatum will eventually give rise to oscillatory activity in the motor cortex that will be traceable using the widefield epifluorescence imaging setup explained in Work Package 1.

To this end, once appropriate functional identified injection site coordinates in the dorsal sensorimotor putamen will be identified, we will microinject bicuculline (50 nM, 10 mM), a GABA<sub>A</sub>R receptor antagonist, to disinhibit and consequently increase the excitability of the target site. Recordings will start over 15 minutes after drug application. For data analysis, averages of 10 trials with 10 sec intervals will be used, unless otherwise required.

### **Work Package 3:** Data analysis

**Objectives:** Reveal aspects of self-organization principles in the motor cortex network dynamics at rest. Determine the effect of striatal inhibition on the motor cortex spatiotemporal output response. Characterize the functional role of CaMKII $\alpha$ + and PV+ neurons in generating spontaneous oscillatory activity.

**Description:** Two distinct mainstreams of analysis, data learning and functional connectome analysis will be combined to offer a multifaceted picture of the motor cortex output response profile. Such a profile will be compared both across repetitions and following striatal disinhibition via bicuculline microinjection. Data pre-processing will include photobleaching artifact removal, temporal band-pass filtering within [1 50] Hz based on the 3<sup>rd</sup> order Butterworth filter (applied in zero-phase mode) and the z-score transformation of the recorded signals. The latter will be applied, independently, to the trace associated with each pixel by using the corresponding mean and standard deviation of signal values recorded before bicuculline microinjection in the dorsal sensorimotor putamen and will give rise to the multisite optical signal, based on which our analysis will be carried out.

Frames of the multisite optical signal will be considered at particular latencies  $t_i$  as an instantaneous activation pattern  $\mathbf{X}(t_i) \in \mathbb{R}^{n \times m}$ , where the pair  $(n, m)$  corresponds to the coordinates of a particular pixel on the imaged plane. In turn, the sequence formed when letting  $t$  span the recording interval will be considered as a dynamical trajectory in a high dimensional space. To get some insights into the involved

dynamics, we will resort to the multi-dimensional scaling (MDS) technique in order to approximately sketch the trajectory in a low-dimensional space. Additionally, based on temporal patterning similarity, the response manifold will be segmented into distinct functional modules and a 2D scatterplot reflecting the inter-module dependencies will be derived. A detailed description of this methodology can be found in (Laskaris et al, 2008) and (Nakajima et al., 2021). Finally, following a network perspective methodology (Nakajima et al., 2021; Antoniadis, 2023) the functional network will be reconstructed and characterized across several recording conditions via estimation and comparison of three well-known network metrics. To alleviate challenges that will be faced at the level of signal analysis, such as data volume, the need for multiple comparisons and the lack of reference response, recent efficient solutions from the fields of machine learning and big data analytics, such as deep learning machines and autoencoders (Bank et al., 2020), will be invoked in the project's framework in association with advances from complex network analytics, such as multilayer networks (Bianconi, 2018). Data analysis will be performed using Neuroplex, MATLAB, and Python.

#### **Work Package 4: Results dissemination**

**Objectives:** Disseminate the project's results through publications in high-profile neuroscience journals and presentations in scientific meetings. Establish close international collaboration with laboratories employing research on the mechanisms of DBS.

**Description:** The results of this project are expected to have a significant impact on the international neuroscience community as they will establish a robust experimental framework upon which future studies seeking to advance our understanding of the therapeutic mechanisms of DBS can rely on. Preliminary results will be presented in national and international conferences. Depending on timing, suitable venues include, but are not restricted to, the Hellenic Society for Neuroscience, FENS Forum, FENS FRM Meetings, SfN Meetings, and DBS Think Tank Meetings. During these meetings, interactions with other groups working in the field of neuromodulation or interested in our approach will be sought to explore the possibilities for future collaborations. Full results will be submitted for publication in international peer-reviewed journals, with appropriate acknowledgement of the funding source.

#### ***Bibliography***

Antoniadis, S. (2023). Analyzing spontaneous oscillatory activity and network organization in cortical slices using the genetically encoded voltage indicator ArcLight. Master Thesis.

Baker, B.J. et al. (2007). Three fluorescent protein voltage sensors exhibit low plasma membrane expression in mammalian cells. *J. Neurosci. Methods*, 161, pp. 32-38.

Bando, Y. et al. (2019). Comparative evaluation of genetically encoded voltage indicators. *Cell Rep.*, 26, pp. 802-813.

Bank, D. et al. (2020). Autoencoders. *arXiv*, arXiv:2003.05991.



- Baumgartner, A. et al. (2022). Novel targets in deep brain stimulation for movement disorders. *Neurosurg. Rev.*, 45(4), pp. 2593-2613.
- Benabid, A.L. et al. (1987). Combined (Thalamotomy and Stimulation) stereotactic surgery of the vim thalamic nucleus for bilateral Parkinson disease. *Appl. Neurophysiol.*, 50, pp. 344-346.
- Benabid, A.L. et al. (2005). Functional neurosurgery for movement disorders: a historical perspective. *Prog. Brain Res.*, 175, pp. 379-391.
- Bernstein, A.J. and Peters, K.M. (2005). Expanding indications for neuromodulation. *Urol. Clin. North Am.*, 32, pp. 59-63.
- Bianconi, G. (2018). *Multilayer networks: structure and function*. OUP.
- Borden, P.Y. et al. (2017). Genetically expressed voltage sensor ArcLight for imaging large scale cortical activity in the anesthetized and awake mouse. *Neurophotonics*, 4(3), 031212.
- Castro-Alamancos, M.A. (2000). Origin of synchronized oscillations induced by neocortical disinhibition in vivo. *J. Neurosci.*, 20, pp. 9195-9206.
- Daigle, T.L. et al. (2018). A suite of transgenic driver and reporter mouse lines with enhanced brain-cell type targeting and functionality. *Cell*, 174, pp. 465-480.
- Delaloye, S. and Holtzheimer, P.E. (2014). Deep brain stimulation in the treatment of depression. *Dialogues Clin. Neurosci.*, 16(1), pp. 83-91.
- Han, Z. et al. (2014). Mechanistic studies of the genetically encoded fluorescent protein voltage probe arclight. *PLoS One*, 9(11). p. e113873.
- Jin, L. et al. (2012). Single action potentials and subthreshold electrical events imaged in neurons with a fluorescent protein voltage probe. *Neuron*, 75(5), pp. 779-785.
- Laskaris, N. et al. (2008). A manifold learning approach to understanding and characterizing olfactory responses from optical recordings. *IEEE Eng. Med. Biol.*, 27, pp. 69-79.
- Lee, S. et al. (2016). Imaging membrane potential with two types of genetically encoded fluorescent voltage sensors. *J. Vis. Exp.*, 4:e53566.
- Liu, X. et al. (2022). Review of noninvasive or minimally invasive deep brain stimulation. *Front. Behav. Neurosci.*, 15.
- Lozano, A.M. and Hamani, C. (2004) The future of deep brain stimulation. *J. Clin. Neurophysiol.*, 21, pp. 68-69.
- Malvea, A. et al. (2022). Deep brain stimulation for Parkinson's disease: a review and future outlook. *Biomed. Eng. Lett.*, 12(3), pp. 303-316.
- Madisen, L. et al. (2015). Transgenic mice for intersectional targeting of neural sensors and effectors with high specificity and performance. *Neuron*, 85, pp. 942-958.

- Marceglia, S. et al. (2017). Adaptive brain stimulation (Adbs) for tourette syndrome. *Brain Sci.*, 8(4).
- McCairn, K.W. et al. (2009). The neurophysiological correlates of motor tics following striatal disinhibition. *Brain*, 132, pp. 2125-2138.
- McCairn, K.W. et al. (2016). A primary role for nucleus accumbens and related limbic networks in vocal tics. *Neuron*, 89, pp. 300-307.
- Milosevic, M.M. et al. (2020). In vitro testing of voltage indicators: ARchon1, Arclightd, Asap1, Asap2s, Asap3b, Bongwoori-Pos6, Berst1, Flicr1, and Chi-Vsfp-Butterfly. *eNeuro*, 7.
- Nakajima, R. et al. (2016). Optogenetic monitoring of synaptic activity with genetically encoded voltage indicators. *Front. Synaptic Neurosci.*, 8(22).
- Nakajima, R. et al. (2021). GEVI cell-type specific labelling and a manifold learning approach provide evidence for lateral inhibition at the population level in the mouse hippocampal CA1 area. *Eur. J. Neurosci*, 53(9), pp. 3019-3038.
- Platisa, J. et al. (2022). Voltage imaging in the olfactory bulb using transgenic mouse lines expressing the genetically encoded voltage indicator ArcLight. *Sci. Rep.*, 12(1).
- Rhee, J.K., Iwamoto, Y. and Baker, B.J. (2021). Visualizing oscillations in brain slices with genetically encoded voltage indicators. *Front. Neuroanat.*, 15.
- Shimaoka, D. et al. (2019). The impact of bilateral ongoing activity on evoked responses in mouse cortex. *Elife*, 8.
- Song, C. et al. (2018). Cortical signatures of wakeful somatosensory processing. *Sci. Rep.*, 8(1).
- Worbe, Y. et al. (2009). Behavioral and movement disorders induced by local inhibitory dysfunction in primate striatum. *Cereb. Cortex*, 19, pp. 1844-1856.
- Worbe, Y. et al. (2013). Towards a primate model of gilles de la tourette syndrome: anatomo-behavioural correlation of disorders induced by striatal dysfunction. *Cortex*, 49, pp. 1126-1140.

## Budget

<b>BUDGET</b>		
<b>Category</b>		<b>Total in €</b>
<b>Direct Costs Personnel</b>		
<b>Post-Doc Researcher(s)</b>		<b>108,000</b>
<b>PhD Candidate(s)</b>		<b>54,000</b>
<b>Total Direct costs for Personnel</b>		<b>162,000</b>
<b>Other Direct Costs</b>	<b>Justification</b>	
<b>6.1.2 Consumables</b>	Laboratory glassware, bicuculline methochloride (25mg)	<b>1000</b>
<b>6.1.3 Travel</b>	Traveling and accommodation, registration fees, training programs and workshops	<b>20,000</b>
<b>6.1.4 Dissemination</b>	Publication fees, conference posters	<b>5,000</b>
<b>6.1.5 Use and/or Access to equipment etc.</b>	2x MATLAB individual academic license, PCR- based genotyping,	<b>2,000</b>
<b>6.1.6 Equipment</b>	2x personal computers	<b>5,000</b>
<b>6.1.7 Other Costs</b>		
<b>6.1.8 Purchase of animals</b>	3x Ai86 (TITL-ArcLight), 3x Camk2a-tTA, 3x Camk2a-Cre, 3x PV-Cre	<b>22,000</b>
<b>Total "other direct costs"</b>		<b>55,000</b>
<b>Total Direct Costs</b>		<b>162,000</b>
<b>Indirect Costs (Institution overhead, 10%)</b>		<b>21,700</b>
<b>Total Budget</b>		<b>238,700</b>

## Short CV



# Spyridon Antoniadis

☎ +30 698 787 2795 | ✉ spirsanto@gmail.com | 📄 spirsanto

Address	Hohenwaldstraße 38 61449 Steinbach (Taunus) Germany
Nationality	Greek
Date of Birth	18/01/1994

## Education

### Master of Science in Neuroscience

NATIONAL AND KAPODISTRIAN UNIVERSITY OF ATHENS

Sep. 2020 - June 2023

Athens, Greece

- Master's degree – EQF level 7
- Major in Neuroscience
- GPA: 8.72/10 – 120 ECTS

### Diploma in Electrical & Computer Engineering

ARISTOTLE UNIVERSITY OF THESSALONIKI

Sep. 2012 - Dec. 2019

Thessaloniki, Greece

- Integrated Master's degree – EQF level 7
- Major in Telecommunications Engineering
- GPA: 7.69/10 – 61 courses, 306 ECTS

### High School Diploma

4TH HIGH SCHOOL OF LARISSA

June 2012

Larissa, Greece

- University Admission Grade: 18.37/20 (top 8%)

## Experience

### Data Scientist / Researcher

LABORATORY OF PHYSIOLOGY, SCHOOL OF MEDICINE, ARISTOTLE UNIVERSITY OF THESSALONIKI

Apr. 2022 - May 2023

Thessaloniki, Greece

Analyzing spontaneous oscillatory activity and network organization in cortical slices using the genetically encoded voltage indicator ArcLight

- Big Data Acquisition & Mining
- Developed intelligible pipelines allowing for connectomic analysis
- Oral and written communication of findings to different types of audience
- Collaboration with the Korea Institute of Science and Technology (KIST)
- Work supported by Hellenic Foundation for Research & Innovation (HFRI-FM17-286)

### Computational Neuroscientist / Researcher

DENDRITES LABORATORY, FOUNDATION OF RESEARCH AND TECHNOLOGY-HELLAS

Sep. 2021 - Mar. 2022

Thessaloniki, Greece

Illuminating the role of calcium-dependent plasticity in memory formation using detailed biophysical models of the hippocampal area CA1

- Model conceptualization based on experimental findings
- Large-scale computational modeling & subsequent data analysis
- Collaboration with Columbia University
- Work supported by National Institutes of Health (NIH-1R01MH124867-01)

### Data Scientist / Researcher

LABORATORY OF PHYSIOLOGY, SCHOOL OF MEDICINE, ARISTOTLE UNIVERSITY OF THESSALONIKI

Apr. 2018 - Jul. 2020

Thessaloniki, Greece

Developing efficient methodologies for gaining insights to calcium imaging datasets.

- Developed intelligible pipelines allowing for exploratory and multivariate pattern data analysis
- Revealed aspects of self-organization principles via statistical inference
- Oral and written communication of findings to different types of audience
- Collaboration with the Korea Institute of Science and Technology (KIST)

## Undergraduate Researcher

SCHOOL OF ELECTRICAL & COMPUTER ENGINEERING, ARISTOTLE UNIVERSITY OF THESSALONIKI

Nov. 2017 - Apr. 2018

Thessaloniki, Greece

- Designed a high accuracy R-R peak detection algorithm for the clinical evaluation of patients suffering from arrhythmia, using Time-Frequency Analysis methods
- Designed a signal analysis pipeline that applied Linear and Non-Linear Time Series Analysis methods for the clinical evaluation of patients suffering from vertigo
- Work confirmed existing publications

## Relevant Training

---

### Deep Learning Specialization

DEEPLARNING.AI & COURSERA

Jun. 2020 - Aug. 2020

## Skills

---

### Operating Systems

Linux (Ubuntu-based), macOS, Microsoft Windows

### Programming Languages

Python (Scikit-learn, TensorFlow, PyTorch, Keras), R, SQL

### Database Platforms

PostgreSQL, MySQL

### Tools

git, MATLAB,  $\LaTeX$ , Microsoft Office, CorelDRAW

### Languages

English (IELTS band 8, Dec. 2019 – CEFR C1)

French (Sorbonne C1, Oct. 2008 – CEFR C1)

German (basic knowledge)

Greek (Native language)

## Volunteering

---

### National Electrical & Computer Engineering Student Conference

ARISTOTLE UNIVERSITY OF THESSALONIKI

Fundraising & Logistics coordinator

Sep. 2013 – Apr. 2014

Thessaloniki, Greece

## Selected Coursework

---

### Neuroscience

Neurobiological Basis of Diseases of the Nervous System, Neuropsychopharmacology, Gross and Microscopic Anatomy of the Nervous System, Computational Neuroscience

### ECE

Biomedical Engineering, Pattern Recognition, Advanced Signal Processing Techniques, Digital Signal Processing, Time Series Analysis, Linear Signals and Systems, Stochastic Signal Processing, Theory of Computation, Information Theory, Probability and Statistics, Automatic Control Systems, Electronics